Journal of Power Sources 238 (2013) 492–500

Contents lists available at SciVerse ScienceDirect

Journal of Power Sources

journal homepage: www.elsevier.com/locate/jpowsour

Using hydroxylamine as a reducer to prepare N-doped graphene hydrogels used in high-performance energy storage

Yunzhen Chang, Gaoyi Han*, Jinping Yuan, Dongying Fu, Feifei Liu, Sidian Li

Institute of Molecular Science, Key Laboratory of Chemical Biology and Molecular Engineering of Education Ministry, Shanxi University, Taiyuan 030006, China

HIGHLIGHTS

- N-doped graphene hydrogels (NGHs) were prepared by thermally treating graphene oxide.
- The optimum conditions were determined by using hydroxylamine as reducing agent.
- The capacitor assembled by the optimum NHGs exhibit good capacitive performance.

ARTICLE INFO

Article history:
Received 2 March 2013
Accepted 16 April 2013
Available online 20 April 2013

Keywords:
Graphene
Hydrogel
N doping
Supercapacitor

ABSTRACT

Solvothermal method is used to obtain N-doped graphene hydrogels (NGHs) using hydroxylamine hydrochloride or hydroxylamine (HA) as the chemical reductant and dopant. During the process, N-doping and reduction of graphene oxide have been achieved simultaneously. The products have been characterized by X-ray diffraction, X-ray photoelectron, Raman spectroscopy and electrochemistry. The results show that the electrical conductivity, microstructure and doping level of NGHs are influenced by the type and quantity of reductants, temperature and time of the reaction. Their capacitive behavior has been investigated by cyclic voltammetry, galvanostatic charge/discharge and electrochemical impedance spectroscopy in an alkaline electrolyte using the two-electrode symmetric capacitor test. The NGHs prepared at 150 °C for 12 h using HA as reductant (NGH–HA12) has N-doping level of 4.32% in atom and exhibits a specific capacitance of 205 F g^{-1} and good cycling stability. The energy density and power density can reach to 3.65 W h kg^{-1} and 20.5 kW kg^{-1} at a discharge of 100 A g^{-1} for the symmetric capacitor assembled using NGH–HA12.

1. Introduction

Supercapacitors, also called electrochemical capacitors, are such kind of electrical devices with high power density (*P*) and energy density (*E*), ultra-long cycle life and low maintenance cost, which make them serve as promising candidates in such fields as portable electronic products, memory back-up systems and hybrid electric vehicles [1–4]. Generally, there are two types of supercapacitors based on the charge-storage mechanism: electrical double layer capacitors (EDLCs) and pseudocapacitors. Moreover, these two mechanisms may function simultaneously based on the nature of the materials.

It is proved that the capacitance of a device depends largely on the characteristics of the materials of electrode. As to materials of electrode, there are three main types: metal oxides, polymeric materials and carbon-based materials, in which the former two undergo a redox reaction to store charge in the bulk of the material and thereby increase the stored energy, but the lower rate of charge/discharge, poor durability and the high cost will limit their further applications [5–8]. Carbon-based materials such as nanoporous carbons [9], carbon nanotubes (CNTs) [10] and graphene [11] have been actively investigated for using as the electrodes of supercapacitors because of their relatively low cost, high chemical stability and environmental friendliness. Besides the focus on the CNTs and other carbon materials, graphene [12] as a new kind of carbon material constructed by a single layer of sp^2 bonded carbon in a hexagonal lattice has shown immense practical advantages due to its high surface area, excellent conductivity and relatively low cost of production. However, as an independent energy storage device, the low intrinsic capacitance of graphene sheets (GSs) cannot fully meet the demand of commercial applications. It has proved that the capacitive behavior of GSs can be further improved

* Corresponding author. Tel.: +86 351 7010699; fax: +86 351 7016358.
E-mail address: han_gaoyis@sxu.edu.cn (G. Han).

0378-7753/$ – see front matter © 2013 Elsevier B.V. All rights reserved.
http://dx.doi.org/10.1016/j.jpowsour.2013.04.074

by chemical doping or etching, in this way, both the presence of the electro-active species and surface area of the pores can contribute to the total specific capacitance [13].

Among the numerous potential dopants, N is considered to be an excellent element because it is of comparable atomic size and contains five valence electrons available to form strong valence bonds with C atoms. So it can be introduced into the lattice of carbon easily to improve the specific capacitance and cycle stability of N-doped graphene (NDG) sheets [14]. Up to now, the approaches including chemical vapor deposition [15], segregation growth [16], arc-discharge [17] and plasma treatment [14,18] have been used to synthesize NDG. However, the above-mentioned N-doping approaches are complex, performed under harsh conditions accompanied by low-yields and high-cost. Recently, several solution-phase processes have been designed to scale up the production of NDG. Besides that the widely-used hydrazine hydrate is used as reducing reagent to prepare graphene from graphene oxide (GO) [19,20]. Lai et al. [21] have synthesized NH_2–graphene by a one-pot process using ethylene glycol as solvent and ammonia as N precursor, and NDG has also been obtained through hydrothermal method by using ammonia or urea as the chemical dopant [13,22]. Hydroxylamine (HA) and its salt, for example hydroxylamine hydrochloride (HACl), exhibit reductive, lower explosive and toxic properties. However, to date, there has been no report on N-doping and reduction of graphene oxide achieved simultaneously using hydroxylamine and its salt as the chemical reductant and dopant.

We present here a simple solvothermal process to achieve N doping and GO reducing simultaneously by using HA or HACl as reducer and dopant in the mixture of ethanol and water for the first time. The obtained products have been characterized and their capacitive behavior is investigated in detail. It is found that this method can provide high quality NDG for applications in energy storage.

2. Experimental section

2.1. Materials

Natural graphite powder (NGP, 325 mesh) was purchased from Tianjin Guangfu Research Institute. HACl was obtained from Tianjin North Fine Chemical Co., Ltd., and all other chemicals used in this study were of analytical grade. HA was generally prepared through the reaction of equimolar HACl with KOH in ethanol solution and used instantly. In a typical procedure, 2.0 mL ethanol solution of HACl (35 mg mL^{-1}) and 1.0 mL ethanol solution of KOH (56 mg mL^{-1}) were mixed, then the mixture was centrifugated at 12,000 r min^{-1} for 3 min to remove the deposition after the mixture was placed at room temperature for 30 min, finally, the ethanol solution of HA with a concentration of 11 mg mL^{-1} was reserved.

2.2. Preparation of the N-doped graphene hydrogels (NGHs)

GO was prepared by oxidation of NGP according to the method reported in the literature [23]. The suspension of GO was prepared by dispersing the as-prepared GO powder into water with the help of ultrasonication. For preparation of NDG used in the measurements of the electric conductivity, 2.0 mL ethanol solution of HACl or HA with different molar concentrations (0.0075, 0.015, 0.05, 0.1, 0.25 and 0.33 mol L^{-1}) was added into 6.0 mL suspension of GO (0.33 mg mL^{-1}) in the small bottles, respectively. After ultrasonication for 5 min, the small bottle containing the reactant was placed into Teflon-sealed autoclave and then heated at 30–175 °C for about 0.5–12 h in an oven. Then the obtained NGHs were dispersed into 200 mL water under ultrasonic condition for 15 min after the autoclave was naturally cooled to room temperature. Subsequently, the suspension was filtered by a mixed cellulose ester filter membrane and the filtration film was dried in air for the electrical conductivity measurement and other structural characterizations.

The representative NGHs for the measurement of capacitive behaviors were prepared via a solvothermal reaction of GO aqueous solution (6 mL, 0.33 mg mL^{-1}) and ethanol solution of HACl or HA about (2 mL, 0.25 mol L^{-1}) at 150 °C for 2 and 12 h. The obtained NGHs were immersed into water for several times to remove the residual reducing agents completely. The obtained hydrogels prepared by HACl or HA at 150 °C for 2 and 12 h were defined as NGH–HACl2 and NGH–HACl12 or NGH–HA2 and NGH–HA12, respectively.

2.3. Characterizations

The NGHs were freeze-dried for characterization. The microstructure of the NGHs was observed on a JEOL-JSM-6701 field-emission scanning electron microscope (SEM) operating at an accelerating voltage of 10 kV. X-ray diffraction (XRD) patterns were recorded on a D8 Advance (Bruker) X-ray diffractometer with Cu Kα radiation ($\lambda = 1.5406$Å) in the 2θ range of 10°–80°. The electrical conductivities were measured by using the standard four-probe technique. X-ray photoelectron spectroscopy (XPS) measurements were performed with an ESCAl-ab220i-XL spectrometer (VG Scientific, England) using a monochromic Al Kα source at 1486.6 eV. Raman spectra were recorded on a JobinYvon Lab RAMHR800 microscopic confocal Raman spectrometer by using laser of 514 nm as incident light.

2.4. Fabrication of the supercapacitors

The fabrication of the supercapacitors is described as follows: two nearly identical (in weight and size) NGHs with the thickness of about 1.0 mm were separated by a filter paper soaked with 25% KOH aqueous solution. Before the electrochemical measurements, the slices of NGHs were also immersed in 25% KOH aqueous solution under vacuum in order to exchange their interior water with electrolyte. Two Pt foils were used as the current collectors. All the components were assembled into a sandwiched structure between the two plastic sheets, the schematic image of the NGHs-based supercapacitor devices are shown in SFig. 1.

2.5. Electrochemical measurements

The assembled two-electrode capacitors were used to measure the performance of NGHs as the electrodes of supercapacitor in an alkaline electrolyte. Electrochemical performances of the cells were tested by cyclic voltammetry (CV), galvanostatic charge/discharge and electrochemical impedance spectroscopy (EIS) on a CHI660C electrochemistry workstation (Chenhua, Shanghai). The potential windows for the CV measurements and galvanostatic charge/discharge tests ranged from −0.5 to 0.5 V. EIS tests were carried out in the frequency range of 10^5 to 0.01 Hz at the amplitude of 5 mV referring to open circuit potential.

In order to analyze the variation of capacitance with varying scanning rates, the specific capacitance (C_{sc}) of the electrodes can be calculated based on CV curves [24] according to following equation:

$$C_{sc} = \left(\int I\mathrm{d}V\right) \Big/ (\nu m \Delta V) \quad (1)$$

where I is the response current (A), ΔV the difference of potential during the CV tests (V), ν the potential scan rate (V s^{-1}), and m the mass of one electrode (g).

Furthermore, the C_{sc}, power density and energy density can also be calculated from the galvanostatic charge/discharge curves [25]. For example, the C_{sc} can be obtained by using the equation:

$$C_{cs} = 2(I\Delta t/m\Delta V) \quad (2)$$

where I represents the constant discharge current, Δt the discharging time, m the mass of one electrode, and ΔV the voltage drop upon discharging. Then the energy density and power density of the EDLCs depicted in the Ragone plot can be calculated by using the equations:

$$E = (1/8)C_{cs}\Delta V^2 \quad (3)$$

$$P = E/\Delta t \quad (4)$$

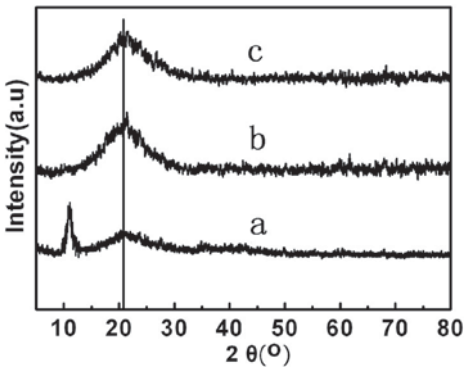

Fig. 2. The XRD patterns of GO (a), NGH–HA2 (b) and NGH–HACl2 (c).

3. Results and discussion

3.1. The characterization of the samples

Fig. 1A shows the relationship between the electrical conductivity of the NDG prepared at 150 °C for 3 h and the concentration of the reducing reagent of HA and HACl. It is found that the conductivity of the NDG prepared by using HA as reducer is smaller than that by using HACl as reducer when the concentrations of the reductant are less than 0.1 mol L^{-1} during the solvothermal reaction. But the contrary result is observed when the concentration of the reducing reagent is greater than or equal to 0.1 mol L^{-1}. For example, the electrical conductivity of NDG can reach to about 3.58 (using HACl as reducer) and 4.98 S cm^{-1} (using HA as reducer) when the concentration of the reductant is 0.25 mol L^{-1}. The influences of the reaction temperatures and time on the electrical conductivity of NDG–HACl and NDG–HA are shown in Fig. 1B and C. It shows that the maximum electrical conductivity is obtained when the reactions are carried out at 150 °C (Fig. 1B). The conductivity of the NDG increases when the reactions are carried out less than 2 h (Fig. 1C), but decreases slightly when the reactions last for more than 2 h.

From Fig. 2 which displays the XRD patterns of GO, NGH–HACl2 and NGH–HA2, it is clear that the XRD pattern of GO shows two diffraction peaks at 11.09° and 21.41° which correspond to the interplanar spacing of 7.97 and 4.15 Å according to the Bragg equation ($2d \sin \theta = n\lambda$). The interplanar spacing of 7.97 Å is consistent with the apparent thickness of a GO's single layer observed by AFM (SFig. 2) while the broad peak at 21.41° indicates that the GO sheets exhibit some aggregations. However, the peak at 11.09° has entirely disappeared after the GO is reduced to NDG, and a broad diffraction peak located at 21.42° is observed in the synthesized NGH–HACl2 and NGH–HA2, which indicates that the interplanar distance of the NDG layers has become small due to the decrease of the oxygen-containing groups. The distance between the layers is calculated to be about 4.14 Å and is still larger than that of graphite (3.35 Å) although it is much smaller than that of GO. This result indicates that the recovery of π-conjugated structure from GO sheets upon solvothermal reduction and the presence of residual oxygenated functional groups on the sheets make the interplanar distance of NDG still larger than that of graphite [25].

The SEM images show that all NGHs possess a 3D network with randomly-oriented porous structure (Fig. 3) which is similar to those found in the literature [26,27], and that the sizes of pores range from sub-micrometer to several microns. It is obvious that the size of the NGHs prepared by 12 h becomes smaller (SFig. 3) than that by 2 h, no matter HACl or HA as reducer, which may imply that the microstructure becomes more compact. It is interesting that NGH–HA2 and NGH–HA12 show the thinner wall formed by overlapping of flexible GSs with more compact structure (smaller size of pores) than NGH–HACl2 and NGH–HACl12. This unique 3D morphology can effectively prevent GSs from restacking caused by force of Van der Waals and interaction of π–π, which is beneficial to electron-transfer and adequate contact with electrolyte.

As a powerful tool to identify the elements' states in material [28], XPS is used to characterize the elemental composition of samples prepared under various conditions. The GO shows obvious O but no N signal in the XPS spectrum (Fig. 4A-a). However, it is visible that there are clear N signals in the XPS spectrum after the GO reacts with HA or HACl for 2 and 12 h (Fig. 4A-b–e). This result is different from the previous report [29] in which the N atom is not doped into the GSs when the HA is used as reducing reagent, and this may come from the higher reaction temperature or the mixture of water and ethanol used as solvent. The high-resolution C1s XPS spectrum of the as-prepared GO shows the signal of C=C bonds formed by sp^2 carbon at 284.4 eV (Fig. 4B) and the signal of C–C bonds formed by sp^3 carbon at 285.0 eV. The fitted peaks located at

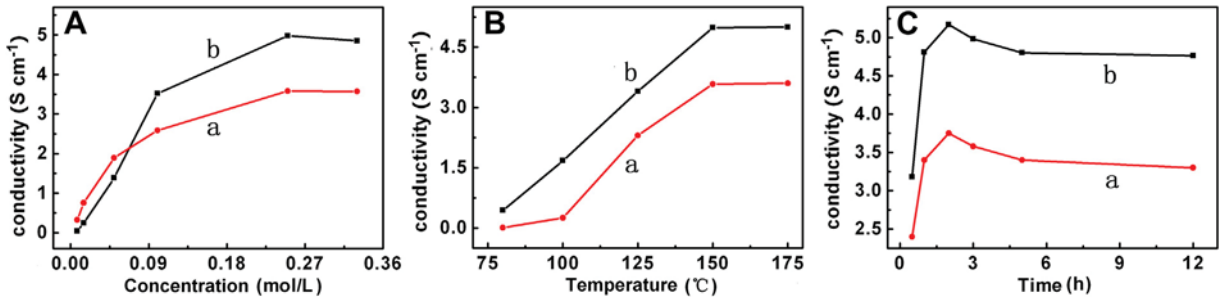

Fig. 1. The plot of electrical conductivity of the NDG prepared by using HACl (a) and HA (b) as reducing reagent versus the molar concentration of the reducing reagent (A), the temperature (B) and the time (C) of the reaction.

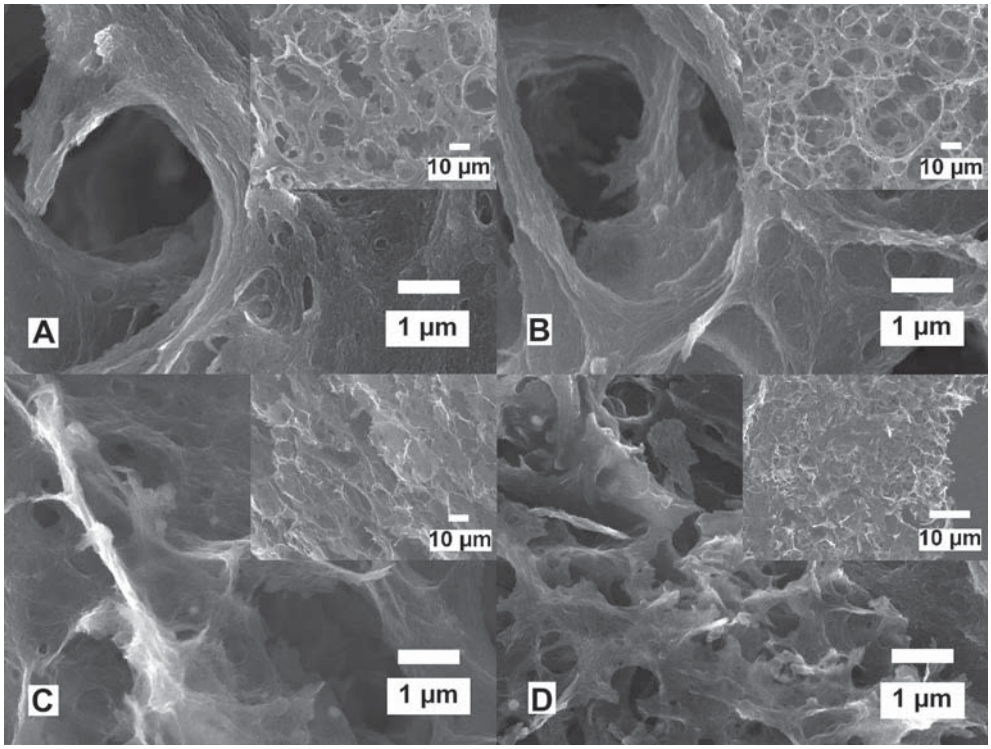

Fig. 3. The SEM images of the NGHs at high and low (insets) magnification, NGH–HACl2 (A), NGH–HACl12 (B), NGH–HA2 (C) and NGH–HA12 (D).

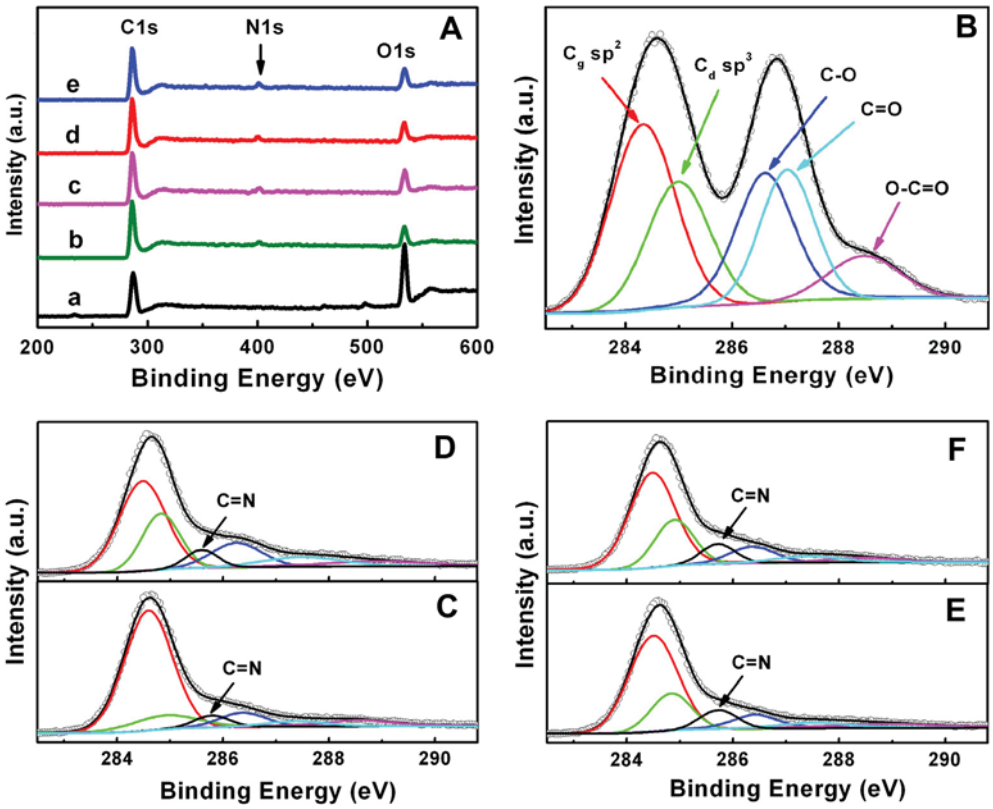

Fig. 4. General XPS spectra of GO, NGH–HACl2, NGH–HACl12, NGH–HA2 and NGH–HA12 (from curves a to e) (A) and high resolution C1s XPS spectra of GO (B), NGH–HACl2 (C), NGH–HACl12 (D), NGH–HA2 (E) and NGH–HA12 (F).

Table 1
The list of the atomic composition of the different samples measured by XPS.

Samples	Elements content (at.%)			Ratios of elements	
	C	O	N	C/O	C/(N + O)
GO	67.3	32.7	0.00	2.06	2.06
NGH–HACl2	84.46	12.86	2.67	6.57	5.44
NGH–HACl12	82.21	14.29	3.50	5.75	4.62
NGH–HA2	84.98	11.84	3.18	7.18	5.66
NGH–HA12	81.70	13.98	4.32	5.84	4.46

Table 2
The relative contents of the different types of N-containing bonds.

Samples	Relative contents of different N (at.%)		
	N1	N2	N3
NGH–HACl2	4.62	74.61	20.77
NGH–HACl12	4.51	85.74	9.75
NGH–HA2	7.71	81.94	10.36
NGH–HA12	8.16	82.33	9.51

higher binding energies are corresponding to large amounts of sp^3 carbon with different C–O bonding configurations. For example, the binding energy related to the groups of C–O, C=O and O=C–O is located at about 286.6, 287.1, and 288.5 eV, respectively [14,30]. However, the intensities of the peaks corresponding to the oxygen-containing groups become much weaker after reaction (Fig. 4C–F), revealing that most of the oxygen-containing groups in GO are removed during the process of the reaction. Significantly, an additional component appears at 285.7 eV, which can be attributed to the C=N bond. It should be noted that the peak of C–N is overlaid by C=O and the peak around 286.5 eV can be assigned to C=O and C–N bonds. All the results mentioned above may demonstrate that NGHs can be successfully prepared by the solvothermal treatment of GO with HACl or HA at 150 °C for 2 h or 12 h [14,22]. The analysis based on Table 1 reveals that the C/O ratio increases obviously from 2.06 to 6.57 or 7.18 after the GO has reacted with HACl or HA for 2 h, but decreases to 5.75 or 5.84 after 12 h. It is also clear that the relative content of N in the NDG–HA is larger than that of NDG–HACl at the same conditions, and that the relative content of N and O increases with the increase of the reaction time. For example, NGH–HA12 possesses the maximum N doping level (4.32%), meanwhile, the O content has increased from 11.84% for NGH–HA2 to 13.98% for NGH–HA12, which may indicate that N-doping can easily occur when the HA is used as the reducing reagent, and that the longer time's reaction makes the defects increase. This result is consistent with that of the electrical conductivity for NDG shown in Fig. 1C.

In order to investigate the possible N insertion pathway in the GSs, the high-resolution N1s XPS spectra of the NDG products prepared at different conditions are collected in Fig. 5. Generally, the peaks located at 398.4, 400.0, and 401.7 eV are assigned to pyridinic-, pyrrolic-, and quaternary-type of N which includes the N doped in the graphene structure and the N in group of R–NH_3^+, respectively [31,32]. The content of various N species is quantitatively depicted in Table 2 based on XPS elemental analysis, which shows that with the increase of solvothermal treatment time, the proportion of quaternary-type of N decreases while the content of pyrrolic N or pyridinic N remarkably increases. It is well known that the following reactions will carry out for HA:

In acid solution:

$$2NH_2OH = N_2 + 2H_2O + 2H^+ + 2e^- \quad (5)$$

$$NH_3OH^+ + 2H^+ + 2e^- = NH_4^+ + H_2O \quad (6)$$

In alkaline solution:

$$2NH_2OH + 2OH^- = N_2 + 4H_2O + 2e^- \quad (7)$$

$$NH_2OH + 2H_2O + 2e^- = NH_3 \cdot H_2O + 2OH^- \quad (8)$$

From the above equations, it is known that HA can be used as reductant and that it can release the ammonia in both acidic and alkaline solution. During the solvothermal process, HA and HACl can be used as reductants to reduce the GO, and the released NH_3 can react with the oxygen-containing groups of GO to form the nitrogen-containing intermediates (e.g. amide and amine) [33] which can undergo dehydration (e.g. pyridine, pyridone) or decarbonylation (e.g. pyrrole) to form relatively stable structures [22,34]. The pyridinic-, pyrrolic-type N increase while the quaternary-type of N decreases when the reaction times reach to 12 h (Table 2), which may be attributed that R–NH_3^+ groups convert to pyridinic- or pyrrolic-type N with the increase of the reaction time. On the other hand, the reactant NH_3 has more reactivity than NH_4^+, so the content of N in the sample of NGH–HA is higher than that in NGH–HACl in the same conditions.

Raman spectroscopy is a convenient method to investigate the graphitic and disordered regions of the carbon materials. The Raman spectra shown in Fig. 6 display a peak at around 1349 cm^{-1} which is attributed to the structural defects and partially disordered structures of the sp^3 domains (D band), while the peak at around 1592 cm^{-1} is assigned to in-plane vibrations of graphite (sp^2-bonded carbon; G band) [35]. The integrated intensity ratios of

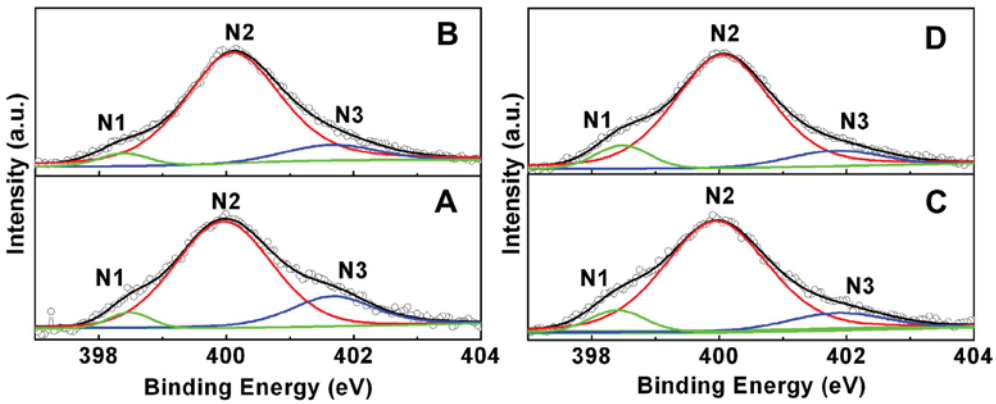

Fig. 5. XPS N1s spectra of NGH–HACl2 (A) and NGH–HACl12 (B) and NGH–HA2 (C) and NGH–HA12 (D) with N1 (pyridinic N), N2 (pyrrolic N) and N3 (quaternary-type N).

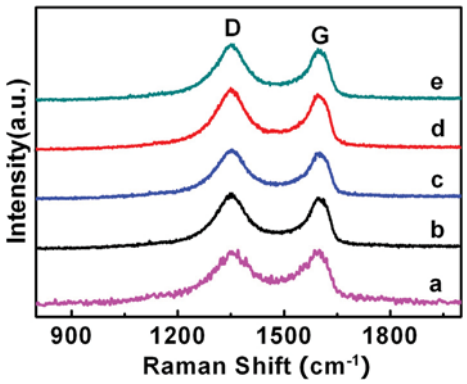

Fig. 6. The Raman spectra of GO (a), NGH–HACl2 (b), NGH–HACl12 (c), NGH–HA2 (d) and NGH–HA12 (e).

the D and G band (A_D/A_G) become larger when GO is reduced to form NGHs, the values of A_D/A_G are about 2.15, 2.27, 2.42, 2.24, 2.3 for GO, NGH–HACl2, NGH–HACl12, NGH–HA2 and NGH–HA12, respectively. The reason may be that the introduction of N especially the "lattice N" which directly bond to in-plane sp^2 bonded carbons will cause the lattice distortion, so the graphitic region transforms into sp^3 domain or numerous sp^2 graphitic domains with smaller sizes [36]. With the increase of the reaction time, the A_D/A_G values increase because of the increase of heteroatom of N and O (Table 1). It is interesting that the A_D/A_G values of NGHs prepared by using HA as reductant are lower than that by using HACl as reductant at the same condition, indicating that the NGH–HA may exhibit larger conjugated domains than NGH–HACl.

3.2. Electrochemical studies on the NGH-based supercapacitors

Cyclic voltammetry method has been used to characterize the capacitor cells assembled by the NGHs-based electrodes and the results are shown in Fig. 7. From the CV curves, it can be seen that the capacitors assembled by the NGH–HACl12 and NGH–HA12 exhibit smaller deviation from the rectangle-like shape than that of NGH–HACl2 and NGH–HA2 at the same scan rates. And it is not found yet that obvious redox waves appear in the CV curves except the appearance of humps in the profiles, which is attributed to the contribution of the redox reactions of the electrochemically active

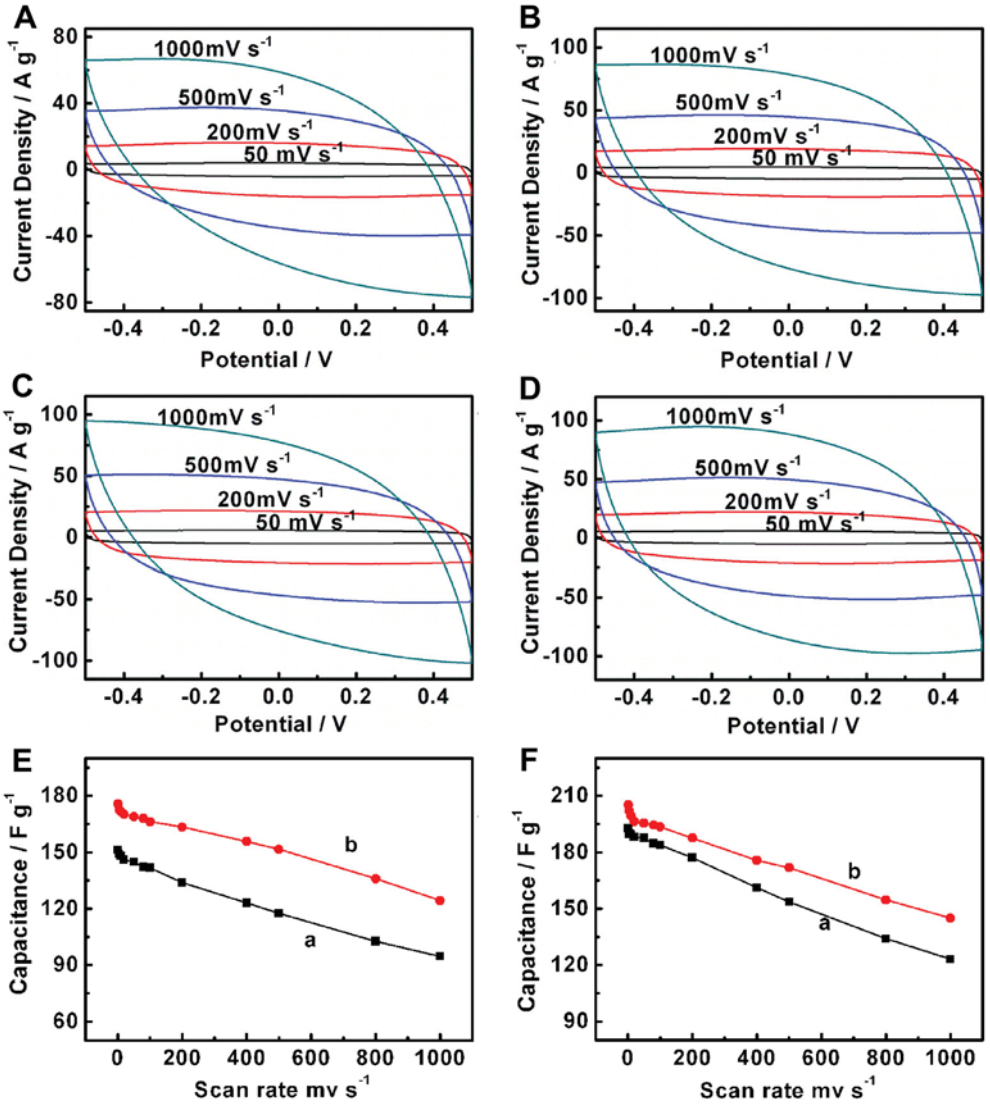

Fig. 7. CV behaviors of the capacitor cells assembled by NGH–HACl2 (A), NGH–HACl12 (B), NGH–HA2 (C), NGH–HA12 (D) and the plots of specific capacitances of the capacitor cell prepared by NGH–HACl2 (E-a), NGH–HACl12 (E-b), NGH–HA2 (F-a), NGH–HA12 (F-b) in 25% KOH electrolyte.

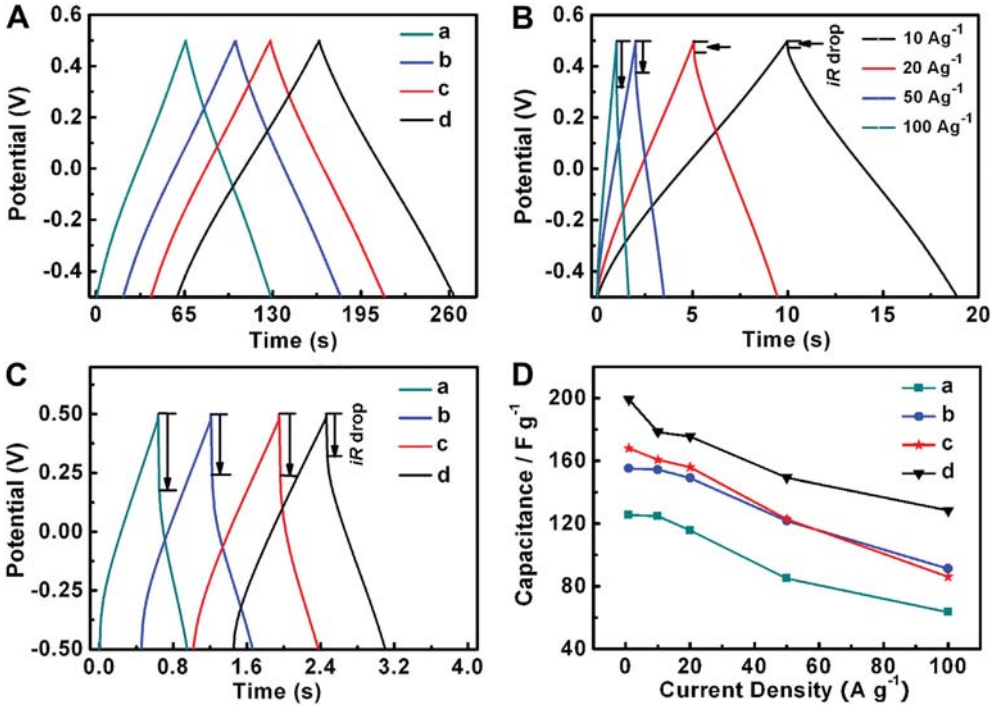

Fig. 8. Galvanostatic charge/discharge curves of the cells assembled by NGHs at current density of 1 (A) and 50 A g^{-1} (C) (in order to see clearly, curves of b–d have been shifted some time backward), charge/discharge curves of the cell assembled by NGH–HA12 at various current densities (B), and the specific capacitance of the NGHs at various discharge current densities (D). In panels A, C and D: NGH–HACl2 (a), NGH–HACl12 (b), NGH–HA2 (c) and NGH–HA12 (d).

functional groups on the surface of the materials, indicating that the electrodes are charged and discharged at a pseudo-constant rate over the whole CV process. Furthermore, we find that the capacitors assembled by NGH–HA2 and NGH–HA12 appear larger current density than that of NGH–HACl2 and NGH–HACl12 at the same scan rates. The C_{sc} of the materials can be calculated based on CV curves and shown in Fig. 7E and F, the capacitor cells assembled by the NGH–HA2 and NGH–HA12 have the C_{sc} values of about 193 and 205 F g^{-1} (Fig. 7F) while the C_{sc} values of the capacitor cells assembled by NGH–HACl2 and NGH–HACl12 are about 151 and 176 F g^{-1} at a scan rate of 1.0 mV s^{-1} (Fig. 7E), respectively.

Furthermore, it is obvious that the C_{sc} values of the NGHs prepared by 12 h are higher at the same scan rate and exhibit slower decreases with the increase of scan rate than that by 2 h, no matter which one is used as reducer, HACl or HA. It's worth noting that the NGH–HA12 not only displays the highest value of C_{sc} at lower scan rate, but also retains higher C_{sc} (70.6% of the initial C_{sc}) at a scan rate of 1000 mV s^{-1} compared with other NGHs-based electrodes.

According to the XPS data listed in Tables 1 and 2, this may be due to the increment of N and O atomic composition in the NDG materials when the reactions last 12 h. It has been reported that the hetero-atoms and functional groups on the GSs can increase the wetting ability of the materials and provide pseudo-capacitance to improve the overall performance of the capacitor [37]. In addition, the fact that C_{sc} value decreases with the increase of scan rate may be due to the limited diffusion on the surface of materials [38].

Fig. 8A shows the charge/discharge curves of the cells prepared by NGHs-based electrodes at current density of 1.0 A g^{-1}, the symmetrical triangles of the charge/discharge plots with small *iR* drops indicate an ideal EDLC behavior of the NGHs-based electrodes and the capacitors assembled by NGH–HA12 shows longer discharge time than the capacitors assembled by other NGHs-based electrodes, which also indicates that electrode NGH–HA12 has better capacitance property than electrode NGH–HACl2, NGH–HACl12, NGH–HA2. Fig. 8B shows the typical galvanostatic charge/discharge curves of the cell assembled by electrode NGH–HA12 at

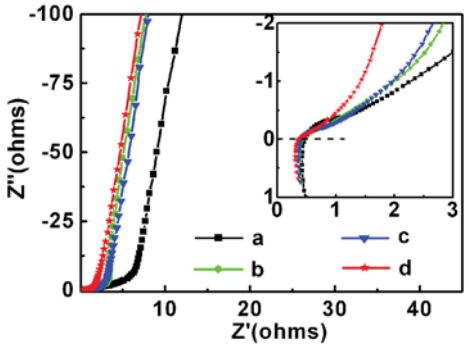

Fig. 9. Nyquist plot of NGH–HACl2 (a), NGH–HACl12 (b), NGH–HA2 (c) and NGH–HA12 (d), and the inset shows the high-frequency region of the plot.

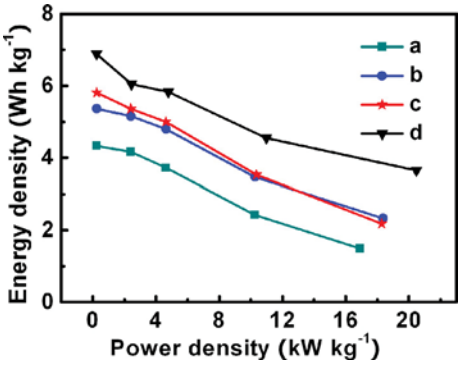

Fig. 10. Ragone plots of the energy density versus power density for the capacitors assembled by NGH–HACl2 (a), NGH–HACl12 (b), NGH–HA2 (c) and NGH–HA12 (d).

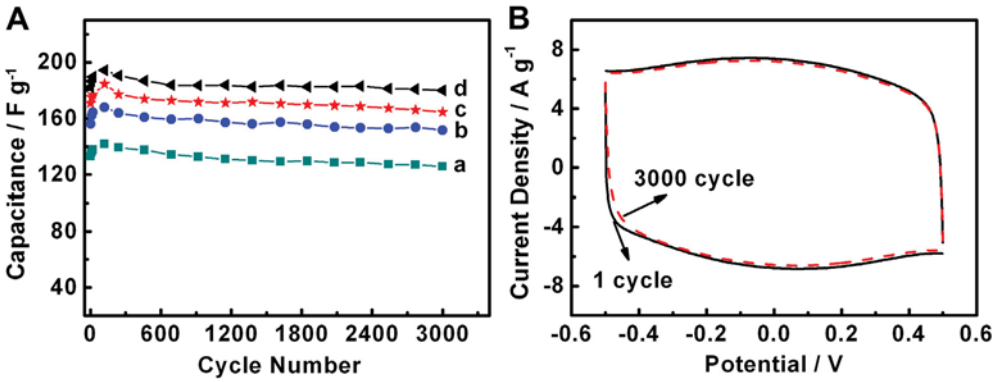

Fig. 11. (A) The relationships between the specific capacitance of the cells assembled by NGH–HACl2 (a), NGH–HACl12 (b), NGH–HA2 (c) and NGH–HA12 (d). (B) The CV curves of the cells assembled by NGH–HA12 under successive CV scan at 80 mV s^{-1}.

current densities of 10, 20, 50 and 100 A g^{-1}, it is found that the *iR* drop increases with the increase of the current density from 10 A g^{-1} to 100 A g^{-1}. Fig. 8C shows the charge/discharge curves of the cells prepared by NGHs-based electrodes at current density of 100 A g^{-1}, it is clear that the cell prepared by NGH–HA12 displays a much lower *iR* drop at the beginning of the discharge process and a longer discharged time. The *iR* drop is usually caused by the overall internal resistance of the devices. Low internal resistance is of great importance in energy-storing devices as less energy will be wasted to produce unwanted heat during charging/discharging processes. It is also found (Fig. 8D) that the C_{sc} values calculated from the discharged curves decrease slightly when the current densities increase, and that the electrode of NGHs–HA12 possesses relatively higher C_{sc} than other electrodes. These results indicate that electrode NGH–HA12 exhibits a rapid current response and excellent capacitive behavior, and that it is more suitable for fabricating safe and power-saving supercapacitors compared with other NGHs.

The kinetic feature of the ion diffusion in the NGHs is also investigated by using EIS technique. Fig. 9 shows the Nyquist plot obtained at the frequency-range of 100,000–0.01 Hz, with an expanded view of the high-frequency region in the inset. The nearly vertical slope of each plot at the low-frequency region indicates a good capacitor behavior of the cells. The negligible high-frequency resistor–capacitor loop shows a good electrode contact [39]. The equivalent series resistances obtained from the Z'-intercept of the Nyquist plot (Fig. 9 inset) show that the capacitor assembled by NGH–HA2 has a smaller resistance than that by NGH–HA2, NGH–HACl12 and NGH–HACl2.

In addition, to validate the promising applications of various NGHs-based electrodes in electrochemical capacitors, the Ragone plot of the symmetric capacitors based on the data of the charge/discharge curves is shown in Fig. 10. The cells of NGH–HA12 possess an energy density of 3.65 W h kg^{-1} when the power density reaches to about 20.5 kW kg^{-1} (excluding the *iR* drop) at the discharging current density of 100 A g^{-1}, which is higher than that of capacitors assembled by NGH–HACl2, NGH–HACl12, NGH–HA2.

As the service life is a very important factor for the electrode of electrochemical capacitor, so the stabilities of the cells assembled by NGH-based electrodes have been evaluated by using CV method at a scan rate of 80 mV s^{-1} (Fig. 11). As can be seen, the specific capacitance of the cells prepared by NGH–HACl2, NGH–HACl12, NGH–HA2 and NGH–HA12 still remained about 88.7, 90.3, 89.13 and 92.6% after 3000 CV charge/discharge processes, respectively. The 92.6% specific capacitance retention over 3000 CV cycles and the curve NGH–HA12 has only a tiny pattern change at the 3000th cycle compared with the 1st CV profile, which illustrate that the material of NGH–HA12 exhibits good durability and may be developed as a suitable material for electrochemical capacitors applications.

4. Conclusions

It is demonstrated for the first time that NGHs can be obtained by using HACl and HA as the chemical dopant and reductant through a simple solvothermal reaction. The NGH–HA12 is tested to be the best material of electrode among the NGHs-based electrode for electrochemical capacitors. The NGH–HA12 has a high C_{cs} of 205 F g^{-1} at scan rate of 1.0 mV s^{-1}, the C_{cs} value can be maintained about 70.6% when the scan rate increases up to 1000 mV s^{-1}, and at the same time it shows a long cyclic life along with about 92.6% of the C_{cs} retention after 3000 cycle tests at a scan rate of 80 mV s^{-1}. Furthermore, the capacitor of NGH–HA12 exhibits an energy density of 3.65 W h kg^{-1} when a power density of 20.5 kW kg^{-1} (excluding the *iR* drop) is achieved at discharging current density of 100 A g^{-1}. The high C_{cs}, power capability at high current density and better cyclic performance may be attributed to its relatively high heteroatom content and the three-dimensional porous structure. The material of NGH–HA12 may be developed as a promising candidate for the next generation of electrochemical capacitors.

Acknowledgments

The authors thank the National Natural Science Foundation of China (21274082 and 21073115) and Shanxi Province (2012021021-3), the Program for New Century Excellent Talents in University (NCET-10-0926) of China and the Program for the Top Young and Middle-aged Innovative Talents of Shanxi province (TYMIT), and the returned personnel of scientific research project of Shanxi (2011-003).

Appendix A. Supplementary data

Supplementary data associated with this article can be found in the online version, at http://dx.doi.org/10.1016/j.jpowsour.2013.04.074.

References

[1] S. Patrice, A.Y. Gogotsi, Nat. Mater. 7 (2008) 845.
[2] E. Frackowiak, F. Beguin, Carbon 39 (2001) 937.

[3] D.A.C. Brownson, D.K. Kampouris, C.E. Banks, J. Power Sources 196 (2011) 4873.
[4] K.X. Sheng, Y.Q. Sun, C. Li, W.J. Yuan, G.Q. Shi, Sci. Rep. 2 (2012) 247.
[5] Y. Zhang, H. Feng, X.B. Wu, L.Z. Wang, A.Q. Zhang, T.C. Xia, H.C. Dong, X.F. Li, L.S. Zhang, Int. J. Hydrogen Energy 34 (2009) 4889.
[6] C.D. Lokhande, D.P. Dubal, O.S. Joo, Curr. Appl. Phys. 11 (2011) 255.
[7] G.A. Snook, P. Kao, A.S. Best, J. Power Sources 196 (2011) 1.
[8] Y.M. Volfkovich, T.M. Serdyuk, Russ. J. Electrochem. 38 (2002) 1043.
[9] V. Khomenko, E. Raymundo-Pinero, F. Beguin, J. Power Sources 195 (2010) 4234.
[10] K.H. An, W.S. Kim, Y.S. Park, J.M. Moon, D.J. Bae, S.C. Lim, Y.S. Lee, Y.H. Lee, Adv. Funct. Mater. 11 (2001) 387.
[11] M.D. Stoller, S. Park, Y.W. Zhu, J. An, R.S. Ruoff, Nano Lett. 8 (2008) 3498.
[12] S. Gilje, S. Han, M.S. Wang, K.L. Wang, R.B. Kaner, Nano Lett. 7 (2007) 3394.
[13] B.J. Jiang, C.G. Tian, L. Wang, L. Sun, C. Chen, X.Z. Nong, Y.J. Qiao, H.G. Fu, Appl. Sci. Res. 258 (2012) 3438.
[14] Y. Wang, Y.Y. Shao, D.W. Matson, J.H. Li, Y.H. Lin, ACS Nano 4 (2010) 1790.
[15] D. Wei, Y. Liu, Y. Wang, H. Zhang, L. Huang, G. Yu, Nano Lett. 9 (2009) 1752.
[16] C.H. Zhang, L. Fu, N. Liu, M.H. Liu, Y.Y. Wang, Z.F. Liu, Adv. Mater. 23 (2011) 1020.
[17] L.S. Panchakarla, K.S. Subrahmanyam, S.K. Saha, A. Govindaraj, H.R. Krishnamurthy, U.V. Waghmare, C.N.R. Rao, Adv. Mater. 21 (2009) 4726.
[18] D.S. Geng, Y. Chen, Y.G. Chen, Y.L. Li, R.Y. Li, X.L. Sun, S.Y. Ye, S. Knights, Energy Environ. Sci. 4 (2011) 760.
[19] D.H. Long, W. Li, L.C. Ling, J. Miyawaki, I. Mochida, S.H. Yoon, Langmuir 26 (2010) 16096.
[20] D.W. Wang, I.R. Gentle, G.Q. Lu, Electrochem. Commun. 12 (2010) 1423.
[21] L.F. Lai, L.W. Chen, D. Zhan, L. Sun, J.P. Liu, S.H. Lim, C.K. Poh, Z.X. Shen, J.Y. Lin, Carbon 49 (2011) 3250.
[22] L. Sun, L. Wang, C.G. Tian, T.X. Tan, Y. Xie, K.Y. Shi, M.T. Li, H.G. Fu, RSC Adv. 2 (2012) 4498.
[23] F.M. Chen, S.B. Liu, J.M. Shen, L. Wei, A.D. Liu, M.B. Chan-Park, Y. Chen, Langmuir 27 (2011) 9174.
[24] Z.J. Fan, J. Yan, T. Wei, L.J. Zhi, G.Q. Ning, T.Y. Li, F. Wei, Adv. Funct. Mater. 21 (2011) 2366.
[25] L. Zhang, G.Q. Shi, J. Phys. Chem. C 115 (2011) 17206.
[26] M.A. Worsley, P.J. Pauzauskie, T.Y. Olson, J. Biener, J.H. Satcher Jr., T.F. Baumann, J. Am. Chem. Soc. 132 (2010) 14067.
[27] K.X. Sheng, Y.X. Xu, C. Li, G.Q. Shi, New Carbon Mater. 26 (2011) 9.
[28] D.X. Yang, A. Velamakanni, G. Bozoklu, S.J. Park, M. Stoller, R.D. Piner, S. Stankovich, I. Jung, D.A. Field, C.A. Ventrice Jr., R.S. Ruoff, Carbon 47 (2009) 145–152.
[29] X.J. Zhou, J.L. Zhang, H.X. Wu, H.J. Yang, J.Y. Zhang, S.W. Guo, J. Phys. Chem. C 115 (2011) 1957.
[30] Z.D. Huang, B. Zhang, R. Liang, Q.B. Zheng, S.W. Oh, X.Y. Lin, N. Yousefi, J.-K. Kim, Carbon 50 (2012) 4239.
[31] H.B. Wang, T. Maiyalagan, X. Wang, ACS Catal. 2 (2012) 781–794.
[32] C.H. Hsu, P.L. Kuo, J. Power Sources 198 (2012) 83.
[33] R. Arrigo, M. Havecker, S. Wrabetz, R. Blume, M. Lerch, J. McGregor, E.P.J. Parrott, J.A. Zeitler, L.F. Gladden, A. Knop-Gericke, R. Schlogl, D.S. Su, J. Am. Chem. Soc. 132 (2010) 9616.
[34] S. Stankovich, D.A. Dikin, R.D. Piner, K.A. Kohlhaas, A. Kleinhammes, Y. Jia, Y. Wu, S.B.T. Nguyen, R.S. Ruoff, Carbon 45 (2007) 1558.
[35] K.N. Kudin, B. Ozbas, H.C. Schniepp, R.K. Prud'homme, I.A. Aksay, R. Car, Nano Lett. 8 (2008) 36.
[36] C.M. Chen, Q. Zhang, X.C. Zhao, B. Zhang, Q.Q. Kong, M.G. Yang, Q.H. Yang, M.Z. Wang, Y.G. Yang, R. Schlogl, D.S. Su, J. Mater. Chem. 22 (2012) 14076.
[37] G. Lota, K. Lota, E. Frackowiak, Electrochem. Commun. 9 (2007) 1828.
[38] S.H. Aboutalebi, A.T. Chidembo, M. Salari, K. Konstantinov, D. Wexler, H.K. Liu, S.X. Dou, Energy Environ. Sci. 4 (2011) 1855.
[39] L.L. Zhang, X. Zhao, M.D. Stoller, Y.W. Zhu, H.X. Ji, S. Murali, Y. Wu, S. Perales, B. Clevenger, R.S. Ruoff, Nano Lett. 12 (2012) 1806.